Disentangling spectral phases of interfering autoionizing states from attosecond interferometric measurements

Lou Barreau,[1,*] C. Leon M. Petersson,[2,*] Markus Klinker,[2] Antoine Camper,[3] Carlos Marante,[2] Timothy Gorman,[3] Dietrich Kiesewetter,[3] Luca Argenti,[4] Pierre Agostini,[3] Jesús González-Vázquez,[2] Pascal Salières,[1,†] Louis F. DiMauro,[3] and Fernando Martín[2,5,6,‡]

[1] *LIDYL, CEA, CNRS, and Université Paris-Saclay, 91191 Gif-sur-Yvette, France*
[2] *Departamento de Química, Módulo 13, Universidad Autónoma de Madrid, 28049 Madrid, Spain*
[3] *The Ohio State University, Department of Physics, Columbus OH 43210, USA*
[4] *Department of Physics & CREOL, University of Central Florida, Orlando, Florida 32816, USA*
[5] *Instituto Madrileño de Estudios Avanzados en Nanociencia (IMDEA-Nanociencia), Cantoblanco, 28049 Madrid, Spain*
[6] *Condensed Matter Physics Center (IFIMAC), Universidad Autónoma de Madrid, 28049 Madrid, Spain*

(Dated: June 27, 2019)

We have determined spectral phases of Ne autoionizing states from XUV-MIR attosecond interferometric measurements and ab initio full-electron time-dependent theoretical calculations in an energy interval where several of these states are coherently populated. The retrieved phases exhibit a complex behavior as a function of photon energy, which is the consequence of the interference between paths involving various resonances. In spite of this complexity, we show that phases for individual resonances can still be obtained from experiment by using an extension of the Fano model of atomic resonances. As simultaneous excitation of several resonances is a common scenario in many-electron systems, the present work paves the way to reconstruct electron wave packets coherently generated by attosecond pulses in systems larger than helium.

Attosecond science has opened the way to real-time observations of electron dynamics in atomic, molecular and condensed-matter systems by providing access to the time scale in which electrons move. In particular, attosecond interferometric techniques, such as the so-called reconstruction of attosecond beating by interference of two-photon transitions (RABBIT) [1–3] originally introduced to demonstrate that XUV pulses produced in high-harmonic generation (HHG) processes come in the form of attosecond pulse trains (APT), have amply been used to investigate electron dynamics in atoms. A very successful example is the determination of atomic photoemission delays [4], both resolved [5, 6] and unresolved [7] on electron emission angle, which has spurred extensive theoretical work [8–12] aimed at establishing the basic concepts supporting this kind of measurements. Past and current extensions of these concepts to more complex systems, such as molecules [13–15] and solids [16–18], or fine-structure dynamics [19], are widening the range of possible applications.

In the above mentioned investigations, the examined photoelectrons were ejected into smooth non resonant continua, i.e., no autoionizing states were populated by the XUV APT and IR pulses used in the interferometric measurements. Under this circumstance, one can make use of Wigner's relationship between photoemission delays and measured spectral phases, as the former vary smoothly with photoelectron energy and can therefore be assigned to the group delay of the moving photoelectron wave packet [12]. This is no longer possible when resonances come into play [20]. In this case, interferometric measurements can still be used to obtain accurate spectral phases and transition amplitudes and hence to reconstruct the electronic wave packet in the vicinity of atomic resonances [21–23]. Such measurements have allowed, for instance, to fully reconstruct a resonant electronic wave packet in helium [22] and to monitor the buildup of the associated Fano profile observed in synchrotron radiation photoionization experiments [24, 25]. A similar buildup of a Fano profile in He has been observed in attosecond transient absorption spectroscopy measurements [26].

So far, experimental reconstruction of electronic wave packets generated in the vicinity of autoionizing states has been limited to isolated atomic resonances, i.e., to the case in which only one of these states is accessible in between two consecutive harmonics. These conditions can easily be met in He [22], where the energy separation between the lowest autoionizing states is quite large, and in more complex atoms, as e.g. Ar [21], when the photon energy is carefully chosen to avoid populating more than one of these states. But in general, many-electron atoms and molecules do not have resonances that separate that much from each other, so the latter circumstance is the exception rather than the rule. On top of that, performing ab initio full-electron time-dependent theoretical calculations for such complex systems, which would be necessary to guide experiments, is very often difficult, if not impossible, since a correct description of the autoionization decay requires an accurate treatment of electron correlation in the continuum. Therefore, finding simple models that may help to disentangle the contributions from different autoionizing states is highly desirable.

In this Letter, we present the results of accurate attosecond interferometric experiments and ab-initio full-

* These authors contributed equally
† pascal.salieres@cea.fr
‡ fernando.martin@uam.es

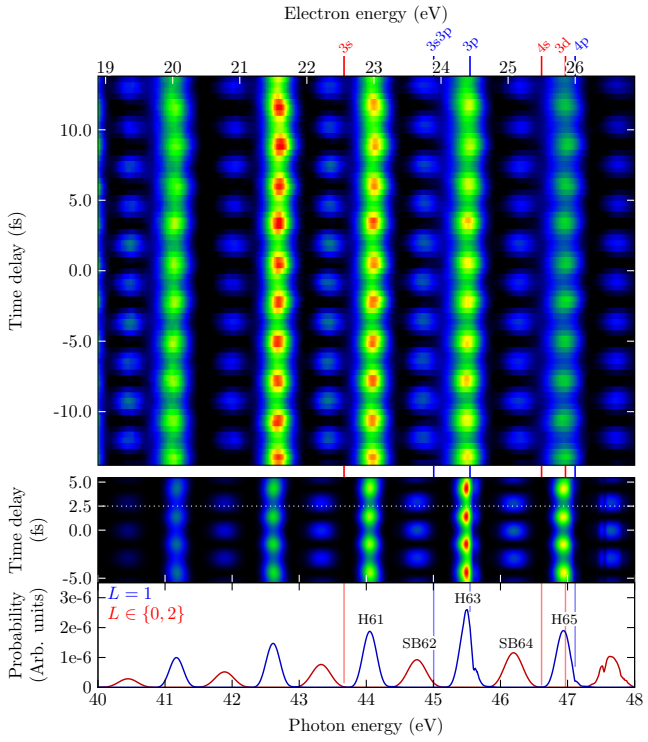

FIG. 1. Measured (upper panel) and TD-XCHEM calculated (central panel) RABBIT spectrograms obtained by using a 1718 nm driving wavelength. In the experiment, 10^4 laser shots are averaged for each delay. The lower panel shows the contributions of states of different symmetries to the calculated photoelectron spectrum for a time delay $\tau = 2.5$ fs. The positions of the Ne resonances are indicated by blue ($^1P^o$ symmetry) and red ($^1S^e$ and $^1D^e$ symmetries) vertical lines.

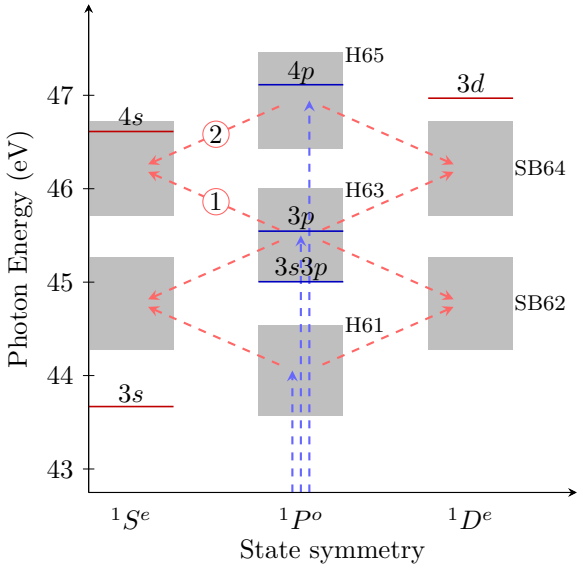

FIG. 2. Energy diagram showing the six lowest resonances of Ne and the relevant ionization channels. Sidebands SB_{62} and SB_{64} result from two-photon interfering paths involving an XUV and a MIR photon (blue and red dashed arrows). Regions scanned in photon energy are shown by shaded areas. The $2s2p^63p\ ^1P^o$ and $2s2p^64p\ ^1P^o$ resonances (denoted $3p$ and $4p$) are populated by harmonics H_{63} and H_{65}, respectively, and can thus interfere through paths ① and ② leading to SB_{64}. The $2s2p^64s\ ^1S^e$ resonance ($4s$) can be populated at the end of these paths. The energy positions and widths of these resonances are $E_{3p} = 45.54$ eV and $\Gamma_{3p} = 16$ meV [25], $E_{4p} = 47.12$ eV and $\Gamma_{4p} = 5$ meV [25], and $E_{4s} = 46.613$ eV and $\Gamma_{4s} = 18$ meV [31]. Values for the other resonances can be found in [31].

electron time-dependent calculations in the vicinity of the $2s2p^63p\ ^1P^o$, $2s2p^64p\ ^1P^o$ and $2s2p^64s\ ^1S^e$ autoionizing states of Ne by using tunable high-order harmonics [21, 27] and a mid infrared (MIR) field of ≈ 1700 nm that efficiently couples these resonances and allows for a fine scanning in photoelectron energy in the region where the autoionization decay occurs. Calculations were performed by using the new time-dependent implementation of the XCHEM methodology [28] (TD-XCHEM), which has been specially designed to accurately describe electron correlation in the ionization continuum of many-electron systems. Measured and calculated photoelectron spectra and sideband phases are in excellent agreement with each other. By using a recent extension of the Fano model to two-photon ionization processes induced by ultrashort pulses [29, 30], we are able to disentangle the contribution of different autoionizing states to the measured phases, which allows one to extract information on individual resonances directly from experiment. This will be crucial to interpret the results of similar experiments performed in more complex systems.

The experiments have been performed on the attosecond beamline at The Ohio State University. In our experimental setup, a 1 kHz repetition rate Ti:sapphire laser (SpitFire) with 12 mJ energy is used to pump an optical parametric amplifier (HE-TOPAS). The 1.5-mJ 60-fs idler pulses around 1700 nm are split into two arms at the entrance of a Mach-Zehnder interferometer with a 8-mm-diameter silver holed mirror. The outer part is focused into a CO_2 gas jet with a $f = 500$ mm lens ($I \approx 1.1 \times 10^{14}$ W/cm^2) for high-harmonic generation. The remaining MIR beam is spatially filtered by an iris. The generated XUV is focused with a toroidal gold mirror in a Ne gas jet in the interaction region of a 1-m-long magnetic bottle electron spectrometer (MBES). The inner part of the beam is delayed by propagating in a glass wedge on a piezoelectric translation and recombined with the XUV on a 6-mm-diameter silver holed mirror. Both beams are spatially and temporally overlapped in the source region of the MBES to induce two-color two-photon ionization. Ne photoelectron spectra were measured as a function of the delay τ between the XUV and the MIR pulses, resulting in the RABBIT spectrogram shown in Fig. 1. A total of sixteen driving wavelengths were used, which allowed us to scan the central energy of the resonant harmonic H_{63} between 45.15 and 45.96 eV.

A sketch of the relevant transitions operating in Ne for the chosen laser parameters is shown in Fig. 2. When

the two-photon XUV-MIR ionization takes place, sideband (SB) peaks appear in between the harmonic peaks in the photoelectron spectrum. The n^{th} sideband signal, resulting from the interference of the absorption of H_{n-1} and absorption of a MIR photon with the absorption of H_{n+1} and stimulated emission of a MIR photon, $S_{\text{SB}}(\tau, n)$, oscillates as a function of the delay τ between the XUV and the MIR pulses at twice the fundamental frequency ω according to:

$$S_{\text{SB}}(\tau, n) = \alpha + \beta \cos[2\omega\tau + \Delta\phi_n + \Delta\bar{\theta}_n^{\text{at}}], \qquad (1)$$

where $\Delta\phi_n = \phi_{H_{n-1}} - \phi_{H_{n+1}}$ is the spectral phase difference between harmonics H_{n-1} and H_{n+1}, and $\Delta\bar{\theta}_n^{\text{at}}$ is the so-called *atomic* phase, corresponding to the phase difference between the two-photon complex transition amplitudes involved $\Delta\bar{\theta}_n^{\text{at}} = \arg\mathcal{A}^{(n-1+1)} - \arg\mathcal{A}^{(n+1-1)}$.

In our scheme (Fig. 2), the $2s2p^6 3p\ ^1P^o$ and $2s2p^6 4p\ ^1P^o$ resonances are reached by absorption of H_{63} and H_{65}, respectively. The $2s2p^6 4s\ ^1S^e$ resonance is accessible by absorption of an additional MIR photon from H_{63} or stimulated emission of a MIR photon from H_{65}. To describe this physical scenario, we have solved the time-dependent Schrödinger equation (TDSE) in the velocity gauge by expanding the time dependent wave function in a basis of Ne eigenstates that includes $^1S^e$, $^1P^o$, $^1D^e$, and $^1F^o$ symmetries, and consists of both bound and continuum states. All Ne eigenstates have been evaluated by using XCHEM [28, 32]. Briefly, continuum states have been evaluated by including four parent ions corresponding to the configurations $1s^2 2s^1 2p^6$ and $1s^2 2s^2 2p^5$, from which neutral states were constructed by augmenting with an additional electron described by both active space orbitals and a hybrid basis of monocentric Gaussian and B-spline functions (GABS basis [33]). The parent ion wave functions were computed by performing a state-average complete active space CAS(7,13) calculation in which all configurations (subject to spin and symmetry restrictions) for seven electrons distributed over the $2s$, $2p$, $3s$, $3p$, $3d$, and $4s$ orbitals, with the $1s$ orbital being doubly occupied always, were included. These orbitals were represented by a standard cc-pVQZ [34] basis of localized gaussian functions. In the GABS basis, the B-splines were chosen to be of order $k = 7$ starting at $R_0 = 7$ a.u. with a node separation of 0.8 a.u. in a box of 2000 a.u., and the monocentric Gaussian functions were built from an even-tempered sequence of 22 exponents (see [32]). After removing the linear dependencies that follow diagonalization of the Hamiltonian, the corresponding TDSE was integrated by using PETSc [35, 36] and the resulting time-dependent wave function was projected onto the corresponding eigenstates. The resulting RABBIT spectrum is shown in Fig. 1.

For computational convenience, the MIR pulse used in the TDSE calculations is shorter than in the experiment (12 vs 60 fs). Thus, comparison with the latter is only meaningful around zero delay, where the APT and MIR pulse overlap significantly. The position of the calculated harmonic bands and sidebands, as well as the frequencies (and as we will see later, the relative phases) of the oscillations are in reasonable agreement with those observed in the measured RABBIT spectrum (see Fig. 1). For a delay of 2.5 fs, the figure also shows the contribution from states of different symmetries to the total photoelectron spectrum. As expected, $^1P^o$ states ($L = 1$) mainly contribute to the harmonic peaks and $^1S^e$ and $^1D^e$ states ($L = 0, 2$) to the sideband peaks. Excitation of the $2s2p^6 3p$ and $2s2p^6 4p\ ^1P^o$ resonances by the XUV field leads to structured H_{63} and H_{65} peaks.

We have extracted spectral phases from both the measured and calculated spectra by summing over the SB spectral width and fitting the resulting oscillations to Eq. 1. In both cases, the harmonic group delay, obtained from a linear fit of the phases of the oscillations as a function of energy [37] excluding the two resonant sidebands, has been subtracted. Its value, $t_e \approx 18$ as/eV, is fairly independent of the driving wavelength in the studied range and is in very good agreement with calculations of the recombination time for the short trajectories using Lewenstein's model [38] in the experimental conditions. The resulting values of $\Delta\bar{\theta}^{\text{at}}$ for SB_{62} and SB_{64} are displayed in Fig. 3. The agreement between our TD-XCHEM calculations and the experiments is excellent. The phase variations are far from trivial, and much less pronounced than in previous work for argon [21] and helium [22] due to the narrowness of the $2s2p^6 3p$ resonance ($\Gamma = 16$ meV) as compared to the harmonics width (≈ 300 meV) and MBES resolution (≈ 250 meV). However, the use of long MIR wavelengths allows for a fine tunability across the resonance and the measurement of such small deviations. As the harmonic energy increases, the atomic phase for SB_{62} smoothly increases by 0.2 rad and then drops to its initial value. For SB_{64}, the phase oscillates with an amplitude of more than 0.1 rad. Due to the small resonance width, no spectral phase variations inside the sidebands were observed using the Rainbow RABBIT analysis [22]. For completeness, Fig. 3 also shows the variation of the photoelectron yield around H_{63} (i. e., in absence of MIR dressing field), which exhibits a typical Fano profile.

An interesting feature of the measured and calculated phases is that, at variance with the results reported for argon [21] and helium [22], the phase variations for SB_{62} and SB_{64} are not mirror images of each other with respect to the zero-phase axis. As shown in [21, 30], approximate mirror images of the spectral phases associated with two consecutive SBs should appear when the corresponding two-photon paths involve a single intermediate resonance and no other resonances are populated in the final state (they would be perfect mirror images if the dipole couplings between the ground state and the non resonant continuum did not depend on energy). This is the consequence of the opposite phase sign of the interfering two-photon transition amplitudes leading to each sideband. Under this circumstance, the phase variation should be very similar to that predicted by the standard Fano model for one-photon transitions. This behavior is observed here for the SB_{62} phase, but not for the SB_{64}

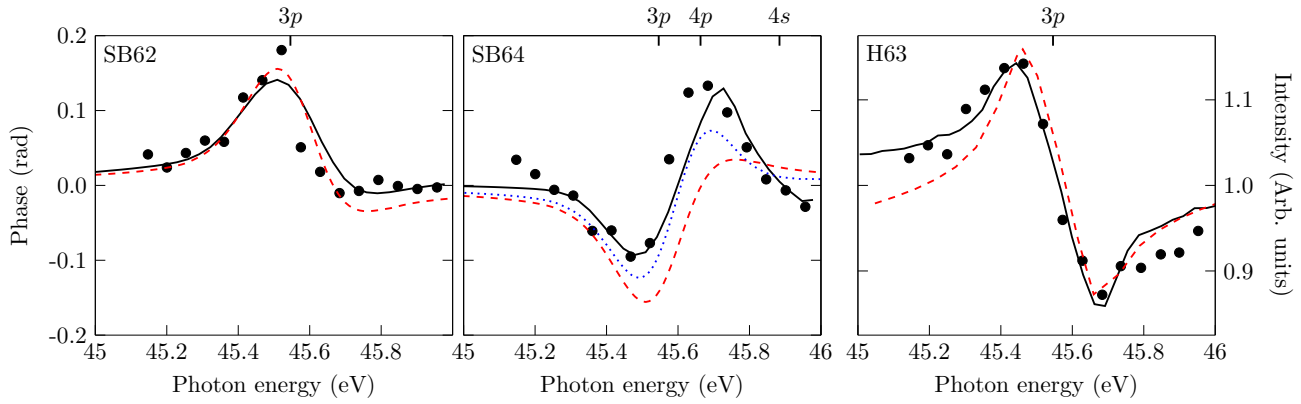

FIG. 3. Measured (full circles) and TD-XCHEM calculated (thick continuous line) atomic phase differences $\Delta\bar{\theta}^{\rm at}$ for SB_{62} (left panel) and SB_{64} (center panel), and normalized H_{63} photoelectron yield (right panel) as a function of the central H_{63} energy. Results of the single-resonance model of Ref. [30] and its generalization to the case of more resonances (Eq. 2) are shown by dashed and dotted lines, respectively. The curves resulting from our TDSE calculations have been shifted up in energy by 0.125 eV to match the position of the $2s2p^6 3p\ ^1P^o$ found experimentally [25]. All shown phases result from spectral integration of the sideband signal.

one. Thus, the absence of such a mirror symmetry can be taken as a first indication of the involvement of more than one resonance.

To get a deeper insight into the physical meaning of the observed phase variations, we have applied an extension of the Fano model for two-photon transitions [30] by assuming that only the $2s2p^6 3p\ ^1P^o$ resonance is populated. Resonance parameters used in this model have been taken from existing synchrotron radiation experiments [25]. Following previous work on He [22] and Ar [21], we have also neglected dipole-induced transitions between the discrete component of the resonance and the adjacent $^1S^e$ and $^1D^e$ non resonant continua, since the corresponding matrix elements are usually negligible (they imply two-electron transitions induced by a one-electron operator). The results of the model are shown as dashed lines in Fig. 3. As can be seen, in spite of its simplicity, the single-resonance model catches the actual phase variations for SB_{62}, showing that only the $2s2p^6 3p\ ^1P^o$ resonance is indeed involved along the two interfering paths leading to this sideband. In contrast, the model fails to reproduce the phase variations for SB_{64}, thus showing that the phase oscillation in this sideband must result from the combined action of the $2s2p^6 3p\ ^1P^o$ and $2s2p^6 4p\ ^1P^o$ resonances.

In order to disentangle the contribution of these resonances to SB_{64}, we use a generalization of the above model as described in [30]. Assuming that, as in the previous case, radiative transitions from the discrete components of the $2s2p^6 3p\ ^1P^o$ and $2s2p^6 4p\ ^1P^o$ resonances to the $^1S^e$ and $^1D^e$ non resonant continua are negligible, and that the $2s2p^6 4s\ ^1S^e$ resonance is not populated, the SB_{64} phases can be written as (by combining Eqs. 7 and 70 of [30] with $\gamma_a = 0$ and using the definition of $\Delta\bar{\theta}_n^{at}$ that follows Eq. 1 above),

$$\Delta\bar{\theta}_{64}^{at}(\omega_f) = \arg\int_{-\infty}^{\infty} d\omega \tilde{\mathcal{F}}_{XUV}(\omega)\,\tilde{\mathcal{F}}_{IR}(\omega_f-\omega)\left[\frac{\varepsilon_{3p}+q_{3p}}{\varepsilon_{3p}+i}\right] - \arg\int_{-\infty}^{\infty} d\omega \tilde{\mathcal{F}}_{XUV}(\omega)\,\tilde{\mathcal{F}}_{IR}(\omega_f-\omega)\left[\frac{\varepsilon_{4p}+q_{4p}}{\varepsilon_{4p}+i}\right] \quad (2)$$

where the first term is associated with path ① in Fig. 2 and the second one with path ②. In this equation, $\epsilon_{np} = 2(E - E_{np})/\Gamma_{np}$, E_{np} being the energy and Γ_{np} the autoionization width of the np resonance, q_{np} is the Fano profile parameter of the np resonance, $\widetilde{\mathcal{F}}_{XUV}(\omega)$ and $\widetilde{\mathcal{F}}_{IR}(\omega_{fg}-\omega)$ are the Fourier transforms of the XUV and IR fields, and ω_f the energy difference between the ground and the final states. All resonance parameters have been taken from experiment [25, 31] (they are in good agreement with those resulting from our XCHEM calculations [32]). The results of the model are shown in Fig. 3 as dotted lines. As can be seen, they are in qualitative agreement with the experimental and the theoretical results. In particular, they show that the contribution of the $2s2p^6 4p\ ^1P^o$ resonance becomes important for photon energies beyond 45.5 eV (referred to the H_{63} central energy), which is the minimum energy required for H_{65} to reach this resonance in the intermediate state. The remaining small discrepancies between the model and the TD-XCHEM results are most likely due to the contribution of the $2s2p^6 4s\ ^1S^e$ resonance not included in the model, although we cannot discard that they are partly due to the basis truncation in the XCHEM calculations. Therefore, by using Eq. 2, we can recover from SB_{64} the phase variation for a pure $2s2p^6 3p\ ^1P^o$ resonance, i.e., without any contamination from other resonances. As expected, this phase variation is close to the mirror image of that extracted from SB_{62}. Of course, in the absence of the $2s2p^6 4p\ ^1P^o$ resonance, one recovers the usual formula for the case of a single resonance. We note that when several non overlapping resonances are populated

by either of the harmonics H_{n-1} and H_{n+1}, extraction of individual phases is still possible by using an expression similar to that given in Eq. 2 by including in each term a sum over the corresponding resonances.

In conclusion, we have determined spectral phases of Ne autoionizing states from XUV-MIR attosecond interferometric measurements and full-electron ab initio calculations in an energy interval where several resonances are involved in the different interfering paths. This is a common scenario in many-electron systems, where several ionization channels are open and resonances lie close to each other, in particular, much closer than the photon energies of consecutive harmonics involved in this kind of measurements. We have found an excellent agreement between measured and calculated phases, thus showing the good performance of the XCHEM method to describe electron correlation in the ionization continuum of these complex systems. As expected, the retrieved phases exhibit a complex behavior as a function of photon energy, which is the consequence of the various resonant contributions to the measured photoelectron spectrum. In spite of this complexity, extracting phases for individual resonances is still possible by using a recent extension of the Fano model to two-photon ionization processes induced by ultrashort pulses [30]. This opens the way to reconstruct resonant electronic wave packets coherently produced in attosecond two-photon ionization experiments performed in complex atoms, thus extending the range of applicability of reconstruction methods as those recently used in the helium atom [39].

ACKNOWLEDGMENTS

Work supported by the ERC proof-of-concept grant 780284-Imaging-XChem within the seventh framework program of the European Union, the MINECO project FIS2013-42002-R, the EU-H2020-LASERLABEUROPE-654148, the ANR projects ANR-15-CE30-0001-CIMBAAD, ANR-11-EQPX0005-ATTOLAB and ANR-10-LABX-0039-PALM, the U.S. Department of Energy, Office of Science, Basic Energy Sciences, under Award no. DE-GF02-04ER15614, and the NSF grant PHY-1607588. Calculations were performed at CCC-UAM and Marenostrum Supercomputer Center. FM acknowledges support from the 'Severo Ochoa' Programme for Centres of Excellence in R&D (MINECO, Grant SEV-2016-0686) and the "María de Maeztu" Programme for Units of Excellence in R&D (MDM-2014-0377).

[1] P. M. Paul, E. S. Toma, P. Breger, G. Mullot, F. Augé, P. Balcou, H. G. Muller, and P. Agostini, Science **292**, 1689 (2001).
[2] H. Muller, Applied Physics B **74**, s17 (2002).
[3] P. Agostini and L. F. DiMauro, Reports on Progress in Physics **67**, 813 (2004).
[4] M. Isinger, R. J. Squibb, D. Busto, S. Zhong, A. Harth, D. Kroon, S. Nandi, C. L. Arnold, M. Miranda, J. M. Dahlström, E. Lindroth, R. Feifel, M. Gisselbrecht, and A. L'Huillier, Science **358**, 893 (2017).
[5] S. Heuser, A. Jiménez Galán, C. Cirelli, C. Marante, M. Sabbar, R. Boge, M. Lucchini, L. Gallmann, I. Ivanov, A. S. Kheifets, J. M. Dahlström, E. Lindroth, L. Argenti, F. Martín, and U. Keller, Phys. Rev. A **94**, 063409 (2016).
[6] C. Cirelli, C. Marante, S. Heuser, C. L. M. Petersson, A. J. Galán, L. Argenti, S. Zhong, D. Busto, M. Isinger, S. Nandi, S. Maclot, L. Rading, P. Johnsson, M. Gisselbrecht, M. Lucchini, L. Gallmann, J. M. Dahlström, E. Lindroth, A. L'Huillier, F. Martín, and U. Keller, Nature Communications **9**, 955 (2018).
[7] M. Schultze, M. Fieß, N. Karpowicz, J. Gagnon, M. Korbman, M. Hofstetter, S. Neppl, A. L. Cavalieri, Y. Komninos, T. Mercouris, C. A. Nicolaides, R. Pazourek, S. Nagele, J. Feist, J. Burgdörfer, A. M. Azzeer, R. Ernstorfer, R. Kienberger, U. Kleineberg, E. Goulielmakis, F. Krausz, and V. S. Yakovlev, Science **328**, 1658 (2010).
[8] L. R. Moore, M. A. Lysaght, J. S. Parker, H. W. van der Hart, and K. T. Taylor, Phys. Rev. A **84**, 061404 (2011).
[9] J. M. Dahlström, T. Carette, and E. Lindroth, Phys. Rev. A **86**, 061402 (2012).
[10] A. S. Kheifets, Phys. Rev. A **87**, 063404 (2013).
[11] J. Feist, O. Zatsarinny, S. Nagele, R. Pazourek, J. Burgdörfer, X. Guan, K. Bartschat, and B. I. Schneider, Phys. Rev. A **89**, 033417 (2014).
[12] R. Pazourek, S. Nagele, and J. Burgdörfer, Rev. Mod. Phys. **87**, 765 (2015).
[13] S. Haessler, B. Fabre, J. Higuet, J. Caillat, T. Ruchon, P. Breger, B. Carré, E. Constant, A. Maquet, E. Mével, P. Salières, R. Taïeb, and Y. Mairesse, Phys. Rev. A **80** (2009).
[14] J. Caillat, A. Maquet, S. Haessler, B. Fabre, T. Ruchon, P. Salières, Y. Mairesse, and R. Taïeb, Phys. Rev. Lett. **106** (2011).
[15] M. Huppert, I. Jordan, D. Baykusheva, A. von Conta, and H. J. Wörner, Phys. Rev. Lett. **117**, 093001 (2016).
[16] A. L. Cavalieri, N. Müller, T. Uphues, V. S. Yakovlev, A. Baltuška, B. Horvath, B. Schmidt, L. Blümel, R. Holzwarth, S. Hendel, *et al.*, Nature **449**, 1029 (2007).
[17] S. Neppl, R. Ernstorfer, A. Cavalieri, C. Lemell, G. Wachter, E. Magerl, E. Bothschafter, M. Jobst, M. Hofstetter, U. Kleineberg, *et al.*, Nature **517**, 342 (2015).
[18] Z. Tao, C. Chen, T. Szilvási, M. Keller, M. Mavrikakis, H. Kapteyn, and M. Murnane, Science **353**, 62 (2016).
[19] I. Jordan, M. Huppert, S. Pabst, A. Kheifets, D. Baykusheva, and H. Wörner, Phys. Rev. A **95** (2017).
[20] L. Argenti, A. Jiménez-Galán, J. Caillat, R. Taïeb, A. Maquet, and F. Martín, Phys. Rev. A **95**, 043426 (2017).
[21] M. Kotur, D. Guénot, Á. Jiménez-Galán, D. Kroon, E. Larsen, M. Louisy, S. Bengtsson, M. Miranda, J. Mauritsson, C. Arnold, S. Canton, M. Gisselbrecht,

T. Carette, J. Dahlström, E. Lindroth, A. Maquet, L. Argenti, F. Martín, and A. L'Huillier, Nat. Commun. **7**, 10566 (2016).

[22] V. Gruson, L. Barreau, Á. Jiménez-Galan, F. Risoud, J. Caillat, A. Maquet, B. Carré, F. Lepetit, J.-F. Hergott, T. Ruchon, L. Argenti, R. Taïeb, F. Martín, and P. Salières, Science **354**, 734 (2016).

[23] D. Busto, L. Barreau, M. Isinger, M. Turconi, C. Alexandridi, A. Harth, S. Zhong, R. J. Squibb, D. Kroon, S. Plogmaker, *et al.*, Journal of Physics B: Atomic, Molecular and Optical Physics **51**, 044002 (2018).

[24] U. Fano, Phys. Rev. **124**, 1866 (1961).

[25] K. Schulz, M. Domke, R. Püttner, A. Gutiérrez, G. Kaindl, G. Miecznik, and C. H. Greene, Phys. Rev. A **54**, 3095 (1996).

[26] A. Kaldun, A. Blättermann, V. Stooß, S. Donsa, H. Wei, R. Pazourek, S. Nagele, C. Ott, C. D. Lin, J. Burgdörfer, and T. Pfeifer, Science **354**, 738 (2016).

[27] M. Swoboda, T. Fordell, K. Klünder, J. Dahlström, M. Miranda, C. Buth, K. Schafer, J. Mauritsson, A. L'Huillier, and M. Gisselbrecht, Phys. Rev. Lett. **104**, 103003 (2010).

[28] C. Marante, M. Klinker, I. Corral, J. Gonzalez-Vazquez, L. Argenti, and F. Martín, Journal of chemical theory and computation **13**, 499 (2017).

[29] A. Jiménez-Galán, L. Argenti, and F. Martín, Phys. Rev. Lett. **113**, 263001 (2014).

[30] Á. Jiménez-Galán, F. Martín, and L. Argenti, Phys. Rev. A **93**, 023429 (2016).

[31] G. Min, Z. Lin-Fan, L. Cun-Ding, and X. Ke-Zun, Chinese Physics Letters **25**, 3646 (2008).

[32] C. Marante, M. Klinker, T. Kjellsson, E. Lindroth, J. González-Vázquez, L. Argenti, and F. Martín, Phys. Rev. A **96**, 022507 (2017).

[33] C. Marante, L. Argenti, and F. Martín, Phys. Rev. A **90**, 012506 (2014).

[34] T. H. Dunning Jr, The Journal of chemical physics **90**, 1007 (1989).

[35] S. Balay, S. Abhyankar, M. F. Adams, J. Brown, P. Brune, K. Buschelman, V. Eijkhout, W. D. Gropp, D. Kaushik, M. G. Knepley, L. C. McInnes, K. Rupp, B. F. Smith, and H. Zhang, *PETSc Users Manual*, Tech. Rep. ANL-95/11 - Revision 3.5 (Argonne National Laboratory, 2014).

[36] S. Balay, W. D. Gropp, L. C. McInnes, and B. F. Smith, in *Modern Software Tools in Scientific Computing*, edited by E. Arge, A. M. Bruaset, and H. P. Langtangen (Birkhäuser Press, 1997) pp. 163–202.

[37] Y. Mairesse, A. de Bohan, L. J. Frasinski, H. Merdji, L. C. Dinu, P. Monchicourt, P. Breger, M. Kovačev, R. Taïeb, B. Carré, H. G. Muller, P. Agostini, and P. Salières, Science **302**, 1540 (2003).

[38] M. Lewenstein, P. Balcou, M. Y. Ivanov, A. L'Huillier, and P. B. Corkum, Phys. Rev. A **49**, 2117 (1994).

[39] C. Ott, A. Kaldun, L. Argenti, P. Raith, K. Meyer, M. Laux, Y. Zhang, A. Blättermann, S. Hagstotz, T. Ding, R. Heck, J. Madronero, F. Martín, and T. Pfeifer, Nature **516**, 374 (2014).